Human Blood-Brain Barrier Endothelial Cells Derived from Pluripotent Stem Cells

Ethan S. Lippmann[1,*], **Samira M. Azarin**[1,*], **Jennifer E. Kay**[1], **Randy A. Nessler**[2], **Hannah K. Wilson**[1], **Abraham Al-Ahmad**[1], **Sean P. Palecek**[1], and **Eric V. Shusta**[1]

[1]Department of Chemical and Biological Engineering, University of Wisconsin-Madison, Madison, WI 53706, USA

[2]Central Microscopy Research Facility, University of Iowa, Iowa City, IA 52242, USA

Abstract

The blood-brain barrier (BBB) plays an important role in brain health and is often compromised in disease. Moreover, as a result of its significant barrier properties, this endothelial interface restricts neurotherapeutic uptake. Thus, a renewable source of human BBB endothelium could prove enabling for brain research and pharmaceutical development. Herein, we demonstrate that endothelial cells generated from human pluripotent stem cells (hPSCs) can be specified to possess many BBB attributes, including well-organized tight junctions, expression of nutrient transporters, and polarized efflux transporter activity. Importantly, hPSC-derived BBB endothelial cells respond to astrocytic cues yielding impressive barrier properties as measured by transendothelial electrical resistance (1450 ± 140 Ωxcm^2) and molecular permeability that correlates well with *in vivo* brain uptake. In addition, specification of hPSC-derived BBB endothelial cells occurs in concert with neural cell co-differentiation via Wnt/β-catenin signaling, consistent with previous transgenic studies. This study represents the first example of organ-specific endothelial differentiation from hPSCs.

INTRODUCTION

The blood-brain barrier (BBB) is composed of specialized brain microvascular endothelial cells (BMECs) that help regulate the flow of substances into and out of the brain. Complex intercellular tight junctions limit the passive diffusion of molecules into the brain and result

in blood vessels exhibiting extremely high trans-endothelial electrical resistance (TEER) *in vivo*[1]. In addition, efflux transporters such as p-glycoprotein contribute to the barrier properties by returning small lipophilic molecules capable of diffusing into BMECs back to the bloodstream. As a result, BMECs are endowed with a requisite network of specific transport systems to shuttle essential nutrients and metabolites across the BBB. In addition, because of its substantial barrier properties, the BBB has significantly hampered neuropharmaceutical development by preventing uptake of the majority of small molecule pharmaceuticals and essentially all biologics[2]. Conversely, BBB breakdown and dysfunction is associated with a variety of neurological diseases, including Alzheimer's disease, stroke, multiple sclerosis, and brain tumors[3]. These issues have collectively led researchers to develop a variety of BBB models to enable detailed mechanistic studies and drug screens *in vitro*.

Most *in vitro* BBB models have been established using brain microvessels isolated from primary animal sources such as cow, pig, rat, and mouse[4]. However, as a result of inevitable species differences[5, 6], a robust *in vitro* BBB model of human origin would be of high utility for conducting high-throughput screening for brain-penetrating molecules or for study of BBB developmental, regulatory, and disease pathways in humans. Previously, human BBB models have been established by culturing primary human BMECs isolated from autopsy tissue, or more often, freshly resected brain specimens derived from tumor or epilepsy patients. As a result, issues involving BMEC availability and fidelity limit the universal use of these human BBB models[7]. Another proposed route toward a human BBB model has been cell immortalization[8]. However, immortalized BMECs suffer from poor barrier properties, including low baseline TEER[8-10] and discontinuous tight junction protein expression[8]. Thus, to create a robust, scalable human BBB model, we sought to take advantage of the *in vitro* developmental potential of human pluripotent stem cells (hPSCs). hPSCs, including both human embryonic stem cells (hESCs)[11] and induced pluripotent stem cells (iPSCs)[12, 13], exhibit virtually unlimited self-renewal and the capacity to differentiate into somatic cell types from all three embryonic germ layers. While human endothelial cells (ECs) have been generated from hPSCs by a variety of methods, including embryoid body differentiation[14-18] and OP9 stromal cell co-culture[19, 20], ECs are known to develop distinct gene and protein expression profiles that depend on microenvironment cues during organogenesis[21], and hPSC-derived ECs with organ-specific properties have yet to be reported. Here we report a facile hPSC differentiation method capable of reproducibly generating pure populations of endothelial cells possessing BBB properties.

RESULTS

Strategy for differentiation of hPSCs into BBB endothelial cells

In vivo, BBB specification begins as ECs forming the perineural vascular plexus invade an embryonic brain microenvironment comprised of neuroepithelial cells, radial glia, neuroblasts, and neurons, and notably much of this early BBB induction occurs in the absence of astrocytes[22-25]. The cells of the developing embryonic brain provide relevant BBB induction cues, such as Wnt7a and Wnt7b, that signal through the canonical Wnt/β-catenin pathway to help promote BBB specification of ECs[26, 27]. We therefore hypothesized

that a strategy which simultaneously co-differentiates hPSCs to both neural and endothelial lineages could result in hPSC-derived ECs possessing BBB attributes. Recent studies have shown that both neural and endothelial cells can be generated from pluripotent stem cells via directed differentiation in adherent culture[28-30]. Thus, we developed a custom 2-dimensional hPSC differentiation strategy that promotes neural and endothelial co-differentiation, in essence providing an embryonic brain-like microenvironment *in vitro*. The strategy was initially implemented using the IMR90-4 iPSC line[13] and protocol robustness was subsequently validated with multiple iPSC and hESC cell lines (Fig. 1a). Briefly, IMR90-4 iPSCs were expanded on Matrigel-coated plates in defined mTeSR1 medium for 2-3 days (Fig. 1a). To initiate neural and endothelial co-differentiation, the colonies were subjected to unconditioned medium (UM) for 3-4 days, at which time large numbers of cells expressing nestin (Fig. 1b [panel i], green), a marker expressed in immature neural progenitors, and βIII tubulin (Fig. 1b [panel i], red), a neuronal marker, were observed. During IMR90-4 iPSC differentiation, 86% of entire cell population could be classified as potential neural progenitors (23% nestin$^+$/βIII tubulin$^-$), immature neurons (58% nestin$^+$/βIII tubulin$^+$) or neurons (5% nestin$^-$/βIII tubulin$^+$), representing a largely embryonic brain-like microenvironment (Fig. 1c). A similar distribution was observed during H9 hESC differentiation (Supplementary Fig. 1a). Within this large immature neural population, very small clusters of cells exhibiting endothelial morphology and PECAM-1 expression, but lacking characteristic BBB tight junctions began to form (Fig. 1d [panel i] and Fig. 1e).

At day 6 of UM treatment, significantly more IMR90-4-derived nestin$^-$/βIII tubulin$^+$ neurons were present (26%) while the nestin$^+$/βIII tubulin$^+$ population decreased to 29% (Fig. 1b [panel ii] and Fig. 1c). By contrast, only small clusters of cells expressing glial fibrillary acidic protein (GFAP; astrocyte marker) and α-smooth muscle actin (α-SMA; potential pericyte/smooth muscle marker) on the order of 30-50 cells per 10^6 could be identified by immunocytochemistry (Supplementary Fig. 2), suggesting that these cells were unlikely to play a major role in BBB specification. Coincident with the maturing neural population at 5-7 days UM treatment, the endothelial regions became larger and more prevalent, and BBB glucose transporter GLUT-1, tight junction proteins occludin and claudin-5, and p-glycoprotein were co-expressed in the endothelial population (Fig. 1f). Although peripheral endothelia are known to express one or more of these markers, the composite set of markers is quite restrictive to brain endothelium[31]. Therefore, the ECs that express tight junction proteins, p-glycoprotein and elevated levels of GLUT-1, will be referred to as hPSC-derived brain microvascular endothelial cells (hPSC-derived BMECs), with further vascular and BBB validation discussed in Figures 3 and 4.

The population of hPSC-derived BMECs was quantified by flow cytometry. For this analysis, BMECs were defined as cells having both PECAM-1 expression and elevated GLUT-1 expression when compared to the low basal GLUT-1 expression exhibited by cells during the first four days of differentiation (GLUT-1$^+$/PECAM-1$^+$, see Materials and Methods for gating details). For IMR90-4-derived BMECs, this population comprised about 30% of the cultures at day 6 of UM treatment (Fig. 1g and Table 1). Thus, the neural and endothelial populations combined represented approximately 95% of the total differentiating culture at day 6 of UM treatment. This hPSC-derived BMEC population was further

expanded for 2 days in a custom EC medium that included factors known to facilitate primary BMEC growth with some selectivity (basic fibroblast growth factor (bFGF) and platelet-poor plasma derived serum[32]), and the percentage of GLUT-1^{+}/PECAM1^{+} cells in the differentiating IMR90-4 culture increased to 66% (Fig. 1d [panel ii], Fig. 1g 6D UM 2D EC, and Table 1). The BMEC differentiation process yielded on average 11.6 PECAM-1^{+}/ GLUT-1^{+} cells per input hPSC after 6 days in UM and 2 days in EC medium, indicating proliferation of EC progenitors and/or ECs during differentiation. At this point, all GLUT-1^{+}/PECAM1^{+} cells co-expressed the requisite BBB markers (Supplementary Fig. 3). Moreover, in EC medium, the hPSC-derived BMECs exhibited a commensurate increase in BBB properties as indicated by substantially increased expression of GLUT-1 protein (Table 1). In contrast, if instead the cultures were grown for two additional days in UM (8 days UM) rather than in EC medium, the percentage of IMR90-4-derived BMECs increased to a lesser extent although the total PECAM-1^{+} population increased to similar levels (Fig. 1g and Table 1), revealing the importance of the EC medium treatment for the selective BMEC expansion and conferral of BBB phenotypes on the EC population. Similar results were observed for the additional iPSC[33] and hESC[11] lines tested (Fig. 1a), with cell line-dependent BMEC differentiation efficiency (Supplementary Figs. 4-6 and Table 1). For the H9 hESC line, extended culture (7 days UM, 6 days EC medium) was required to improve BMEC yield from 16% to 35% of the population (Fig. 1g and Table 1). Thus, in general, 2-dimensional differentiation and expansion of hPSCs for 6-7 days in UM followed by 2-6 days in EC medium generated substantial yields of highly enriched hPSC-derived BMECs.

Involvement of Wnt/β-catenin signaling in hPSC-derived BMEC specification

Murine *in vivo* and *in vitro* studies have demonstrated that canonical Wnt/β-catenin signaling is necessary for the onset of brain angiogenesis and the acquisition of BBB properties such as GLUT-1[26, 27] and claudin-5 expression[34]. Canonical Wnt ligands Wnt7a and Wnt7b have been specifically implicated in BBB development *in vivo* and are expressed by neural progenitors[26, 27]. Therefore, we assayed for *WNT7A* and *WNT7B* expression in the neural progenitor/neuron populations and monitored the temporal nuclear localization of β-catenin in the developing hPSC-derived BMEC population. Nearly all nestin^{+} cells and βIII tubulin^{+} cells (i.e. all three developing neural populations evaluated in Fig. 1c) expressed *WNT7A* and *WNT7B* transcripts at day 4 of UM treatment (Fig. 2a, Supplementary Fig. 1b-j, and Supplementary Fig. 7a). While junctional β-catenin in PECAM-1^{+} ECs was widespread, nuclear β-catenin was sparse at this time (7±4% of PECAM-1^{+} ECs; Fig. 2b [panel i]). By day 6 of UM treatment when large percentages of the culture had adopted a BMEC phenotype, the majority of the nestin[+] and βIII tubulin^{+} cells maintained expression of *WNT7A,* except for some bipotent βIII tubulin^{+} cells (Supplementary Fig. 7b-e), while the *WNT7B* transcript was no longer detected. The percentage of PECAM-1^{+} ECs exhibiting detectable nuclear β-catenin substantially increased to 40±6% at 5 days of UM treatment (Fig. 2b [panel ii]) and nearly all PECAM-1^{+} ECs (90±6%) possessed nuclear β-catenin after 6 days UM and 2 days EC treatment (Fig. 2a [panel iii] and Supplementary Fig. 8 for other hPSC lines). Of note, elevated expression of GLUT-1 was nearly exclusively detected in cells that also contained nuclear β-catenin (Fig. 2b [panel ii]), which is consistent with *in vivo* reports of an absence of BBB GLUT-1 in endothelial-specific β-catenin knockout

mutants[26] and GLUT-1 downregulation in the vascular plexus of *WNT7A/7B* double knockout mutants[27].

Given that all cell lines tested exhibited nuclear β-catenin localization during BMEC differentiation, linkage to Wnt-mediated processes was also assessed by evaluating transcript expression of Wnt receptors and target genes during IMR90-4 differentiation (Fig. 2c). Gene expression levels in later (7D UM) cultures containing ~30% PECAM-1^{+}/ GLUT-1^{+} BMECs and early (3D UM) cultures devoid of these cells were compared. As expected, transcripts indicative of BMEC differentiation, *ABCB1* (p-glycoprotein) and *SLC2A1* (GLUT-1), were upregulated during this time period (Fig. 2c). Wnt receptors Frizzled4 (*FZD4*) and Frizzled6 (*FZD6*) have been implicated in angiogenesis of retinal[35-37] and brain ECs[26], with the *FZD6* transcript being highly expressed in adult brain ECs compared with lung and liver ECs[26]. Transcripts of Frizzled4 and Frizzled6 were upregulated in concert with the emergence of IMR90-4-derived GLUT-1^{+}/PECAM1^{+} BMECs in the differentiating cultures, whereas the *FZD7* gene, which encodes Wnt receptor Frizzled7 that has no known linkage to brain endothelial differentiation[26, 27], was downregulated during this same time frame. The gene products for β-catenin-associated transcription factor *LEF1* and Wnt-downstream gene *FST* (encoding for follistatin) were also upregulated during this time. In addition, the *STRA6* gene, which encodes a BBB-resident vitamin A transporter[38] that has been identified as a Wnt target gene[39] and is enriched in adult brain ECs compared to lung and liver ECs[26], was upregulated during the course of BBB differentiation. *APCDD1*, which has been noted to be highly enriched in adult brain ECs compared to lung and liver ECs[26] and was recently shown to be an antagonist of Wnt signaling[40], remained unchanged over the time course of analysis, potentially suggesting a more prominent *APCDD1* role in adult BBB maintenance through Wnt pathway regulation rather than in BBB development. Treatment with the Wnt signaling inhibitors secreted Frizzled Receptor Protein 2 (SFRP2) or XAV-939 resulted in downregulation of *LEF1, FST, STRA6, FZD6, SLC2A1*, and *ABCB1* (Fig. 2c), further supporting the involvement of Wnt signaling in regulating these transcripts. Moreover, differentiating IMR90-4 cultures treated with XAV-939 exhibited a reduction in GLUT-1^{+} cells from 64% to 46% (Fig. 2d and Table 1). Treatment with XAV-939 also led to a slight reduction in the overall percentage of PECAM-1^{+} cells (68% to 61%), thus giving a 19% net reduction in the overall percentage of PECAM-1^{+} ECs that became PECAM-1^{+}/GLUT-1^{+} BMECs. Interestingly, the presence of XAV-939 did not alter claudin-5 or occludin localization even in GLUT-1^{−} ECs, and western blots indicated equal amounts of claudin-5 and occludin in the differentiating cultures regardless of XAV-939 treatment (data not shown). These data compare favorably with observations in endothelial-specific β-catenin knockout mouse mutants where brain vascular malformations lacked GLUT-1 expression but still possessed tight junctions[26]. Thus, while certain aspects of BMEC specification appear to be influenced by the Wnt-β-catenin pathway (e.g. elevated GLUT-1 expression), this pathway is likely not exclusively responsible for BMEC specification[41-43].

Purification of hPSC-derived BMECs

Although the 2-dimensional co-differentiation strategy resulted in large numbers of hPSC-derived BMECs as defined by expression of tight junction proteins, p-glycoprotein, and

elevated GLUT-1, many characteristic BBB properties, including barrier formation and transporter activity, are best evaluated in purified, confluent monolayers. Furthermore, RT-PCR analysis indicated that the IMR90-4-derived BMECs, while expressing the *PECAM1* transcript, lacked expression of endothelial transcripts encoding for von Willebrand factor (vWF) and VE-cadherin during the early UM treatment phase (Fig. 3a). During EC medium treatment, VE-cadherin expression was detected (Fig. 3a), consistent with sequential expression of PECAM-1 and VE-cadherin endothelial genes previously observed during EC differentiation from stem cells[44]. Thus, to stimulate further maturation and facilitate purification, IMR90-4-derived BMECs were subcultured from Matrigel onto plates coated with collagen/fibronectin extracellular matrix commonly used for primary BMEC culture[32]. In EC medium, the cells grew to confluence after 1-2 days, were contact-inhibited, exhibited characteristic EC morphology (Fig. 3b) and were capable of acetylated low-density lipoprotein uptake (Fig. 3c). Approximately 100% of the cells in the purified cultures expressed PECAM-1 and the requisite BBB markers as judged by flow cytometry and immunocytochemistry (Fig. 3d and 3e), indicating effective and facile purification using this extracellular matrix-based selective passaging method. Importantly, the cells also acquired vWF and VE-cadherin expression during subculture, indicating EC maturation (Fig. 3a and 3e), and vascular character of these BMECs was further confirmed by formation of tube-like structures in the presence of vascular endothelial growth factor (VEGF) (Fig. 3f). The extent of BBB maturation achieved during UM and EC medium treatment prior to subculture onto the fibronectin/collagen matrix was critical for obtaining this pure, confluent monolayer of BMECs. For example, when IMR90-4-derived BMECs were subcultured after just 4 days of UM treatment, cells expressing BBB markers still developed, but did not reach confluence and in many areas showed malformed and discontinuous tight junctions (Fig. 3g). This lack of BBB differentiation correlated well with the observation that at this stage of UM treatment, minimal β-catenin nuclear localization could be found (Fig. 2b [panel i]) and no PECAM-1$^+$/claudin-5$^+$ cells were present (Fig. 1e). Similar purification results were found for DF19-9-11T-derived BMECs when subcultured onto the collagen/fibronectin matrix (Supplementary Fig. 9 and Table 1), while DF-6-9-9T-derived BMECs (Supplementary Fig. 10) could also be purified although they exhibited some discontinuous junctions (Supplementary Fig. 10c). H9-derived BMECs could not be purified away from the large percentage of non-brain PECAM-1$^+$/GLUT-1$^-$ ECs by the collagen/fibronectin protocol given the general affinity of ECs for the collagen/fibronectin matrix. The IMR90-4 and DF19-9-11T lines were therefore used for in-depth BBB phenotype testing as described below.

BBB phenotype of iPSC-derived BMECs

In addition to BBB marker expression and vascular phenotype, iPSC-derived BMECs should also respond to astrocyte cues, exhibit tight barrier properties, and express functional transport systems. A hallmark of the BBB is the high trans-endothelial electrical resistance (TEER) that is a consequence of tight junction protein interactions between adjacent BMECs. To measure the TEER for the BMEC monolayers, IMR90-4-derived BMECs were seeded onto Transwell filters coated with collagen/fibronectin matrix and grown to confluence in EC medium to create a standard two-compartment BBB model (Fig. 4a). Immunofluorescent detection of ZO-1, occludin, and claudin-5 demonstrated the

maintenance of continuous cell-cell contacts between BMECs on the filter surface, similar to the tight junctions observed on fibronectin/collagen-coated polystyrene culture dishes (Supplementary Fig. 11). Initial TEER measurements taken at confluence were 150-175 Ωxcm^2, indicative of a tightening endothelial monolayer (Fig. 4b, time 0h). TEER measurements following co-culture with either primary rat astrocytes or non-neural human embryonic kidney (HEK) 293 cells in EC medium were compared to monocultured IMR90-4-derived BMECs. After 24 hours, TEER in the astrocyte co-cultures (412±38 Ωxcm^2) nearly doubled that observed in both HEK cell co-culture (236±23 Ωxcm^2) and BMEC monoculture (222±51 Ωxcm^2) and remained elevated up to 96 hours, indicating a specific response to astrocyte cues as expected of BMECs (Fig. 4b and Table 2). If astrocyte co-culture was instead performed in medium containing 10% FBS, TEER of the IMR90-4-derived monolayer reached 696±8 Ωxcm^2 after 24 hours, while TEER in the HEK cell co-cultures was again significantly lower at 364±53 Ωxcm^2 (Table 2). Optimization of seeding density to generate a more uniform monolayer yielded IMR90-4-derived BMECs with a maximum TEER of 1450±140 Ωxcm^2 upon astrocyte co-culture (Table 2). DF19-9-11T-derived BMECs exhibited a maximum TEER of 777±112 Ωxcm^2 during astrocyte co-culture (Table 2). The iPSC-derived BMEC monolayers typically exhibited maximum TEER between 24-48 hours of co-culture and maintained elevated TEER levels up to 8 days (Supplementary Fig. 12). In terms of robustness, iPSCs of differing passage number consistently yielded TEER in a range of 700-1450 Ωxcm^2 over the course of thirty individual experiments, with an average value of 860±260 Ωxcm^2. For comparison, one of the highest documented TEER values for primary human BMECs obtained from fresh biopsy is 339±107 Ωxcm^2 (ref. 45) and the immortalized human BMEC cell line, hCMEC/D3, reaches a maximum TEER of 199±5 Ωxcm^2 in response to hydrocortisone[9], whereas peripheral endothelium exhibits a TEER in the 2-30 Ωxcm^2 range.

To further validate the fidelity of the tight junctions formed by the IMR90-4-derived BMECs after co-culture with astrocytes, these cells were subjected to freeze-fracture electron microscopy (Fig. 4c). Freeze-fracture revealed networks of tight junction strands whose complexity mimicked that of high resistance BBB endothelium *in vivo* and the tight junction particles were primarily associated with the protoplasmic fracture face (P-face), favorably contrasting with lower resistance *in vitro* BBB models that oftentimes undergo a switch of tight junction particles from the P-face to the E-face[46].

The BBB *in vivo* is not only characterized by its high TEER, but also by its impermeability to passive diffusion, expression of various transport systems used for import and export of nutrients and metabolites, and its ability to act as an active barrier to small hydrophobic molecules by employing key efflux transporters like p-glycoprotein, breast cancer resistance protein (BCRP), and members of the multidrug resistance protein (MRP) family. Purified IMR90-4-derived BMECs co-cultured with astrocytes expressed transcripts encoding a variety of receptors/transporters found at the BBB (Fig. 4d), such as *LDLR* (low density lipoprotein receptor), *LRP1* (low density lipoprotein receptor-related protein 1), *INSR* (insulin receptor), *LEPR* (leptin receptor), *BCAM* (lutheran glycoprotein), *TFRC* (transferrin receptor), and *AGER* (receptor for advanced glycation endproducts, RAGE). Transcripts were also detected for members of amino acid and peptide transporter families that are

highly enriched at the BBB compared to other endothelium, including *STRA6* (retinol binding protein), *SLC2A1* (GLUT-1), *SLC7A5* (LAT1), *SLC1A1* (EAAT3), *SLC38A5* (SNAT5), and *SLC16A1* (MCT1). Efflux transporter transcripts were also detected, including *ABCB1* (MDR1/p-glycoprotein), *ABCG2* (BCRP), *ABCC1* (MRP1), *ABCC2* (MRP2), *ABCC4* (MRP4), and *ABCC5* (MRP5). Of note, two assayed transcripts were not detected: *PLVAP* and *SLC21A14*. *PLVAP* (plasmalemma vesicle-associated protein) is initially expressed at the BBB during development and becomes downregulated with onset of barrier properties while its expression remains in peripheral vessels throughout adulthood[24]. Thus, the absence of *PLVAP* in the IMR90-4-derived BMECs is a further indicator of BBB specification and maturation. *SLC21A14* (also known as *SLCO1C1*) encodes Oatp14, an organic anion transporter whose transcript and protein product is highly enriched at the rodent but not human BBB[47, 48]. Taken together, the gene expression profile of receptors and transporters is highly representative of the BBB.

Next, radiolabeled small molecules with varying sizes, lipophilicity, and efflux transporter recognition were screened for relative permeability using the IMR90-4-derived BMEC/ astrocyte co-culture model (Fig. 4e and Supplementary Table 1). The measured permeability (P_e) values showed excellent correlation ($R^2=0.98$) to *in vivo* rodent brain uptake measured by *in situ* brain perfusion[49]. Importantly, sucrose permeability ($P_e=3.4\times10^{-5}$ cm/min), which is often used to benchmark the passive barrier of *in vitro* models, was on the order of high-fidelity animal BBB models (10^{-4}-10^{-5} cm/min)[49, 50] and significantly lower than the hCMEC/D3 line ($P_e=1.65\times10^{-3}$ cm/min)[8]. Glucose, a small (180 Da), hydrophilic molecule that is actively influxed across the BBB by the GLUT-1 transporter, accordingly demonstrated a 7-fold higher permeation compared to sucrose ($P_e=2.2\times10^{-4}$ cm/min). Inulin, a large, hydrophilic, polysaccharide polymer, showed similar permeation to sucrose ($P_e=2.9\times10^{-5}$ cm/min). Diazepam, a very lipophilic small molecule that demonstrates high BBB penetration *in vivo* because it is not an efflux transporter substrate, showed the highest *in vitro* permeation (1.1×10^{-3} cm/min). Colchicine and vincristine, which are also lipophilic small molecules but have limited brain uptake *in vivo* since they are substrates of p-glycoprotein and MRP family members, were accordingly found to have lower P_e values *in vitro* (9.2×10^{-5} and 6.2×10^{-5} cm/min, respectively). Prazosin, which is effluxed by BCRP but also thought to be influxed by an organic cation transporter, showed slightly higher P_e (2.9×10^{-4} cm/min) than colchicine and vincristine, correlating to its *in vivo* ranking. Importantly, the 40-fold dynamic range of P_e values (diazepam/sucrose) indicates the potential utility of the iPSC-derived BBB model as a drug screening tool, although future testing with a broader spectrum of compounds will be needed to fully validate the predictive power of the model.

While the relative exclusion of the aforementioned lipophilic small molecules like colchicine, vincristine, and prazosin implies functionality of the relevant BBB efflux transporters described in Figures 3e and 4d, we also assessed their functionality and polarity using selective inhibitors (full compound details found in Supplementary Table 2). First, p-glycoprotein function in monocultured IMR90-4-derived BMECs was probed using rhodamine 123, a cell-permeable, fluorescent p-glycoprotein substrate. There was a 1.4-fold increase in cellular accumulation of rhodamine 123 (decrease in efflux) in the presence of

cyclosporin A, a known p-glycoprotein inhibitor, but not when Ko143 or MK 571, inhibitors of BCRP and the MRP family respectively, were used, indicating the presence of functional p-glycoprotein in IMR90-4-derived BMECs (Fig. 4f [panel i]). When doxorubicin, a substrate for p-glycoprotein, BCRP, and the MRPs, was added to monocultured IMR90-4-derived BMECs, its accumulation was increased in the presence of cyclosporin A, Ko143, or MK 571, demonstrating the functional efflux activity of each class of transporter (Fig. 4f [panel i]). Next, directional transport assays using the IMR90-4-derived BMEC/astrocyte co-culture model were used to demonstrate preferential efflux function in the brain-to-blood direction (basolateral to apical). For p-glycoprotein, transport of rhodamine 123 from the apical to basolateral chamber was 2.3-fold higher in the presence of cyclosporin A, but not Ko143 or MK 571, as a result of inhibited efflux in the basolateral to apical direction (Fig. 4f [panel ii]). Conversely, transport of rhodamine 123 in the basolateral to apical direction slightly decreased upon treatment with cyclosporin A as a result of blocking p-glycoprotein extrusion of rhodamine 123 at the apical interface (Supplementary Fig. 13). Transport of doxorubicin from the apical to basolateral chamber was increased 1.3-fold, 1.3-fold, and 1.2-fold by cyclosporin A, Ko143, and MK 571, respectively, indicating net functional polarization of p-glycoprotein, BCRP and MRP family efflux transporters (Fig. 4f [panel ii]). Together, these data demonstrate both function and polarization of efflux transporters. Importantly, the degree of polarization, as measured by increased flux in the presence of inhibitors, is consistent with that found in primary cultured *in vitro* rodent BBB systems[49]. Overall, the composite of BBB gene and protein expression, tight junction fidelity, correlative permeability for small molecules, and polarized efflux transporter activity benchmarks the iPSC-derived BMECs as possessing significant BBB character.

DISCUSSION

Traditional methods of primary animal and human BMEC culture are employed by a limited number of laboratories because of their complexity. Moreover, primary BMEC culture is hampered by yield constraints. Immortalized cell lines can alleviate yield concerns but are instead limited by their diminished BBB phenotype. In contrast, the approaches described here for generating hPSC-derived BMECs capable of forming robust BBB models are of comparative ease and readily scalable given the efficiency of endothelial differentiation (>60%) and the capability to perform facile extracellular matrix-based purification. By comparison, other hPSC differentiation strategies utilizing embryoid bodies, OP9 co-culture, and 2D differentiation with endothelial factors have lower reported EC differentiation efficiencies (1-43%), and must be coupled with antibody-assisted purification methods to yield pure populations of ECs[14-20, 29, 30]. Also, the differentiation process reported here resulted in a high yield of 11.6 PECAM-1^{+}/GLUT-1^{+} BMECs per input hPSC after 8 days of differentiation whereas recent publications using OP9 co-culture and embryoid body/ directed differentiation methods have reported yields of 0.6 and 7.4 ECs, respectively[15, 19]. Thus, the stem cell basis for this model presents a highly scalable source of human BMECs that, for example, can easily be scaled to generate sufficient cells for thousands of filters for drug screens. In addition, none of these previous approaches has reported an EC population possessing organ-specific properties. In this study, BBB specification occurred in the presence of co-differentiating neural cells, which likely supplied many of the necessary cues

normally provided by the embryonic brain microenvironment *in vivo*[24, 26, 27, 34, 41-43]. It is possible that co-differentiation strategies could also specify ECs of other lineages by providing organ-specific microenvironmental cues during development *in vitro*.

Given that BMEC populations were obtained from both hESC and iPSC lines derived via distinct reprogramming strategies, this hPSC-derived BMEC model could be readily adopted by the broader research community for studies of brain development, disease mechanisms, and drug delivery. The *in vitro* BBB specification process appears to involve Wnt/β-catenin signaling which is consistent with *in vivo* mechanisms of brain development demonstrated in mice[26, 27, 34]. This model could therefore enable the elucidation of other molecular mechanisms leading to human BBB differentiation, studies which is intractable in humans. Information regarding human BBB development could be clinically relevant for promoting BBB repair after stroke or inhibiting recruitment of blood vessels by brain tumors. Having shown the hPSC-derived BMECs possess excellent barrier characteristics with appropriate molecular exclusion and functional transport systems, it is anticipated this cellular platform will also be useful in drug permeability screens to either develop pharmaceuticals that can reach the brain or to limit the brain uptake of drugs that may have neurotoxic side effects.

MATERIALS AND METHODS

hPSC culture and differentiation

Human embryonic stem cells (H9)[11] and induced pluripotent stem cells (iPS(IMR90)-4 (ref. 13), iPS-DF19-9-11T[33], and iPS-DF6-9-9T[33]) were maintained on irradiated mouse embryonic fibroblasts in standard unconditioned medium: Dulbecco's Modified Eagle's Medium/Ham's F12 containing 20% Knockout Serum Replacer (Invitrogen), 1× MEM nonessential amino acids (Invitrogen), 1 mM L-glutamine (Sigma), 0.1 mM β-mercaptoethanol (Sigma), and human basic fibroblast growth factor (bFGF, 4 ng/mL for hESCs and 100 ng/mL for iPSCs; Waisman Clinical Biomanufacturing Facility, University of Wisconsin-Madison). Prior to differentiation, cells were passaged onto Matrigel (BD Biosciences) in mTeSR1 medium (STEMCELL Technologies). After 2-3 days in mTeSR1 (ref. 51), medium was switched to unconditioned medium lacking bFGF (referred to as UM throughout the manuscript) to initiate differentiation. Major morphological changes were observed by day 5-7 of UM treatment, at which point the medium was switched to endothelial cell (EC) medium: human Endothelial Serum-Free Medium (Invitrogen) supplemented with 20 ng/mL bFGF and 1% platelet-poor plasma derived bovine serum[32] (PDS; Biomedical Technologies, Inc.). Following 1-2 days of EC medium treatment, cells were dissociated with dispase (2 mg/mL; Invitrogen) and plated onto 12-well tissue culture polystyrene plates or 1.12 cm^2 Transwell-Clear® permeable inserts (0.4 μm pore size) coated with a mixture of collagen IV (400 μg/mL; Sigma) and fibronectin (100 μg/mL; Sigma). Culture plates were incubated with the coating for at least 30 min at 37 °C, while the inserts were incubated for a minimum of 4 h at 37 °C. One well of differentiated hPSCs from a standard 6-well tissue culture plate (9.6 cm^2) could be used to seed either three wells of a collagen/fibronectin-coated 12-well plate (11.4 cm^2) or four collagen/fibronectin-coated inserts (4.48 cm^2). Cells were then cultured in EC medium until they reached confluence (typically 1-2 days). Over the course of dozens of differentiation and purification

experiments, multiple lots of PDS (5 lots), Knockout Serum Replacer (at least 3 lots), Matrigel (at least 3 lots), collagen IV (new batches every 2-3 months), and fibronectin (new batches every 2-3 months) were used with no observable effects on differentiation efficiency or BMEC barrier fidelity. In addition, it is important to note that none of the aforementioned materials were qualified or prescreened for their capacity to promote efficient differentiation.

hPSC-derived BMEC co-culture experiments

For co-culture experiments, primary astrocytes were isolated as previously described[52]. Briefly, cortices were isolated from P6 neonatal Sprague Dawley rats (Harlan) and minced in Hank's Balanced Salt Solution (HBSS; Sigma). This tissue was digested in HBSS containing 0.5 mg/mL trypsin (Mediatech, Inc.) in a 37 °C shaker bath for 25 min, followed by digestion in HBSS containing 114 U/mL DNase I (Worthington Biochemical) in a 37 °C shaker bath for 5 min. After trituration and filtration, cells were cultured on collagen-I-coated flasks (100 μg/mL; Sigma) in DMEM containing 10% qualified heat-inactivated fetal bovine serum (FBS; Invitrogen), 10% heat-inactivated horse serum (Sigma), 2 mM L-glutamine, and 1% antibiotic-antimycotic (Invitrogen). Human embryonic kidney 293 cells (HEK cells; ATCC) were cultured in DMEM supplemented with 10% FBS, 1 mM sodium pyruvate (Sigma), 2 g/L sodium bicarbonate (Fisher Scientific), 30 mM HEPES (Sigma), and 1% antibiotic-antimycotic, and used as a non-neural cell control. Co-culture of hPSC-derived BMECs was initiated with primary rat astrocytes or HEK cells in either EC medium (called 1% PDS medium in Table 2) or 70:30 (v/v) DMEM/F12 (Sigma/Invitrogen) supplemented with 1% antibiotic-antimycotic, 2% B27 (Invitrogen), and 10% FBS[52] (called 10% FBS medium in Table 2). Trans-endothelial electrical resistance (TEER) measurements were performed using an EVOM voltohmmeter (World Precision Instruments) at the start of co-culture and every 24 h thereafter. The resistance value ($\Omega \times cm^2$) of an empty filter coated with collagen/fibronectin was subtracted from each measurement. To determine the P_e of radiolabeled ligands, compounds were diluted to 0.4 μCi in transport buffer (distilled water with 0.12 M NaCl, 25 mM NaHCO$_3$, 3 mM KCl, 2 mM MgSO$_4$, 2 mM CaCl$_2$, 0.4 mM K$_2$HPO$_4$, 1 mM HEPES, and 0.1% bovine serum albumin [BSA; Sigma]) and 0.5 mL were added to the upper chamber. 200 μL aliquots were extracted from the basolateral chamber every 15 min and replaced by fresh transport buffer. The rate of accumulation of radioactive ligand in the basolateral chamber over the course of 1 h was used to calculate P_e values for [^{14}C]-sucrose, [^{3}H]-inulin, [^{3}H]-colchicine, [^{3}H]-diazepam, [^{3}H]-prazosin, [^{14}C]-glucose, and [^{3}H]-vincristine. [^{3}H]-vincristine was purchased from American Radiolabeled Chemicals, while all other radiolabeled compounds were acquired from PerkinElmer. All compound incubations were conducted at 37 °C, and the radioactive permeability experiments were carried out on a rotator. Triplicate filters were used for all permeability studies.

Efflux transport assays

P-glycoprotein, BCRP, and MRP functionality were assessed using rhodamine 123 (Sigma), a preferred substrate for p-glycoprotein, and [^{14}C]-doxorubicin (PerkinElmer), a substrate for all aforementioned efflux transporters. To assess activity, hPSC-derived BMEC monolayers cultured on polystyrene (absent astrocyte co-culture) were pre-incubated for 30

min on a rotator at 37 °C with or without 5 μM cyclosporin A (Sigma), 1 μM Ko143 (Sigma), or 10 μM MK 571 (Sigma), which are inhibitors of p-glycoprotein, BCRP, or various MRPs, respectively. BMECs were then incubated with rhodamine 123 (10 μM) or doxorubicin (0.25 μCi) for 1 h on a rotator at 37 °C with or without inhibitors. Cells were then washed three times with ice-cold PBS and lysed with 5% Triton X-100 (TX-100; Fisher). Fluorescence (485 nm excitation and 530 nm emission) was measured using a plate reader and normalized to cell counts obtained using a hemacytometer, while radioactivity was measured using a liquid scintillation counter. To quantify apical-to-basolateral transport, hPSC-derived BMEC monolayers on Transwell filters were co-cultured with astrocytes for 24 h and then pre-incubated with or without inhibitors for 60 min, followed by addition of rhodamine 123 or doxorubicin to the upper chamber. After another 60 min, aliquots were extracted from the bottom chamber and transport was quantified on a plate reader or scintillation counter. To quantify basolateral-to-apical transport, hPSC-derived BMEC monolayers on Transwell filters were pre-incubated with or without cyclosporin A for 60 min, followed by addition of rhodamine 123 to the lower chamber. After 3 h, aliquots were extracted from the upper chamber and fluorescence quantified on a plate reader. All measurements of accumulation and transport were normalized to accumulation and transport in the absence of inhibitor. Rhodamine accumulation and transport studies were carried out in the 10% FBS co-culture medium, while doxorubicin studies were conducted in transport buffer described above. Sucrose permeability and TEER measurements were used to confirm monolayer integrity in the presence of inhibitors.

Tube-forming and acetylated low-density lipoprotein (LDL) uptake assays

24-well tissue culture plates were coated with 500 μL of Matrigel for 1 h at 37 °C. Collagen/fibronectin-purified hPSC-derived BMECs were dissociated using trypsin, and 100,000 cells were plated into each Matrigel-coated well in EC medium supplemented with 40 ng/mL VEGF (R&D Systems) and imaged after 12 h. A control sample of cells lacking VEGF was also employed. For acetylated LDL uptake, purified hPSC-derived BMECs were incubated with 10 μg/mL acetylated LDL conjugated to Alexa Fluor 488 (Invitrogen) for 4 h at 37 °C, washed twice with PBS, and visualized immediately with an Olympus epifluorescence microscope. Images were taken using a Diagnostic Instruments camera run by MetaVue software.

Immunocytochemistry/in situ hybridization

Cells were washed once with PBS and fixed in either 2% paraformaldehyde or 100% ice-cold methanol for 15 min. The cells were then blocked with 40% goat serum in PBS (40% PBSG). If probing for an intracellular antigen, 0.1% TX-100 was present in the 40% PBSG. The cells were then incubated in 40% PBSG containing primary antibodies (see Supplementary Table 3 for list) for 1 h at room temperature or overnight at 4 °C. After three washes in PBS, cells were incubated in 40% PBSG containing goat anti-rabbit Texas Red (1:500; Invitrogen) or goat anti-mouse Alexa Fluor 488 (1:500; Invitrogen) for 1 h at room temperature. Cell nuclei were labeled with 300 nM 4′,6-Diamidino-2-pheny-lindoldihydrochloride (DAPI) for 10 min. Cells were washed three times in PBS and visualized. Vascular and BBB markers were tested at the time points indicated in the Results text. Markers characteristic of basal epithelial and epithelial progenitor cells, cytokeratin

K14 and the p63 transcription factor, were tested in IMR90-4 derived cells after 6 days of UM and 2 days of EC medium treatment or in purified IMR90-4-derived BMECs and were not detected. The simple epithelial cytokeratin K18 was expressed in undifferentiated IMR90-4 iPSCs and its expression was still detected in all cells of the mixed differentiating population after 6 days of UM and 2 days of EC treatment. *In situ* hybridization for detection of *WNT7A* and *WNT7B* transcripts was conducted similar to the method described by Planell-Saguer *et al*[53]. Briefly, cells were washed once with PBS and fixed in 2% paraformaldehyde for 10 min, followed by permeabilization in PBS containing 0.1% TX-100 for 5 min. Pre-hybridization was performed with a water-based solution containing 3% BSA and 4× saline-sodium citrate buffer (SSC; Fisher), followed by a 1 h hybridization in 4× SSC and 10% dextran sulfate (Fisher) at room temperature. Digoxigenin (DIG)-labeled locked nucleic acid probes were purchased from Exiqon and DIG-labeled locked sense probes were used as negative controls (sequences found in Supplementary Table 4). Following three washes in 4× SSC/0.1% Tween-20, one wash in 2× SSC, one wash in 1× SSC, and one wash in PBS (all washes conducted at 50 °C), cells were blocked in PBS containing 4% BSA for 20 min and labeled overnight at 4 °C with a monoclonal anti-digoxigenin antibody (Sigma). Secondary antibody and DAPI labeling were carried out as described above.

Flow cytometry

Cells were harvested via Accutase (Invitrogen) incubation for 2-3 min, fixed in 100% ice-cold methanol for 20 min, and blocked with 40% PBSG for 20 min at room temperature. Primary antibody labeling (Supplementary Table 3) was performed in 10% PBSG for 1 h at room temperature. IgG controls were used at the same concentration. After a wash with 5% FBS in PBS, secondary antibodies (goat anti-rabbit Alexa Fluor 488 and goat anti-mouse Alexa Fluor 647; 1:200) in 10% PBSG were added to each sample for 30 min at room temperature. After two washes with 5% FBS in PBS, the samples were analyzed on a FACScaliber flow cytometer. For quantification purposes, PECAM-1$^+$ events were quantified using a PECAM-1/forward scatter dot plot referenced to a rabbit IgG control. Events demonstrating elevated GLUT-1 expression (GLUT-1$^+$) were quantified using a GLUT-1/forward scatter dot plot referenced to a 4D UM culture that lacked BMECs to account for low basal GLUT-1 expression in the differentiating culture. Events that were found in both of these positive gates were classified as PECAM-1$^+$/GLUT-1$^+$ cells. PECAM-1$^+$ events having basal GLUT-1 expression were referred to as PECAM-1$^+$/GLUT-1$^-$. For inhibition of BMEC differentiation, 10 μM of XAV-939 (Sigma)[54] or equivalent DMSO vehicle control was added to IMR90-4 iPSCs starting at day 2 of UM treatment, and PECAM-1/GLUT-1 expression were evaluated as described above. Data are presented as two-dimensional dot plots with color codes for ease of viewing. βIII tubulin and nestin expression were quantified against rabbit and mouse IgG controls, respectively, using two-color flow cytometry.

Reverse-transcription polymerase chain reaction (RT-PCR), quantitative RT-PCR, and gel electrophoresis

Cells were differentiated as previously described. For inhibition of Wnt signaling, cells were treated with 250 ng/mL of mouse secreted frizzled-related protein 2 (SFRP2; R&D

Systems)[55] in UM for 4 days, followed by 750 ng/mL of SFRP2 in UM for an additional 3 days, or with 10 μM XAV or equivalent volume of DMSO vehicle control starting at day 2 of UM treatment. For RNA collection, cells were washed once with PBS and dissociated with trypsin or accutase. Total RNA was extracted using an RNeasy Mini Kit (Qiagen) according to the manufacturer's instructions. cDNA was generated from 1 μg of RNA using Omniscript reverse transcriptase (Qiagen) and oligo-dT primers (Invitrogen). Quantitative PCR (qPCR) was then performed using 1 μL of cDNA and iQ SYBR Green Supermix (Bio-Rad) on an iCycler (Bio-Rad). RT-PCR was also performed using GoTaq Green Master Mix (Promega). Primer sequences are supplied in Supplementary Table 4. Relative expression was quantified using the comparative cycle threshold (C_T) method, normalizing to glyceraldehyde-3-phosphate dehydrogenase (*GAPDH*) expression. Fold difference was calculated as $x^{-\Delta\Delta CT}$, where x refers to primer efficiency calculated according to LinRegPCR version 12.3 (ref. 56). Transcript amplification was analyzed by 2% agarose gel electrophoresis of the qPCR or RT-PCR products.

Freeze-fracture electron microscopy

After 24 h of co-culture with rat astrocytes, IMR90-4-derived BMECs were washed once with PBS, fixed in 1.5% glutaraldehyde (Sigma) for 60 min, washed several times with PBS, cryoprotected with glycerol (30%), scraped from the filters, loaded into gold specimen carriers (Bal-Tec part # LZ 02125 VN), and plunged in liquid ethane. Frozen specimens were transferred to a Balzers 301 Freeze Fracture Apparatus for fracturing and 1 min of sublimation at −110 °C. Etched fracture surfaces were replicated with platinum at 45° supported by carbon deposited from 90°. Replicas were cleaned for 1 h using commercial household bleach followed by rinsing with double distilled water. Bare 400 mesh copper grids were used to pick up the cleaned replicas. Images were obtained using a JEOL 1230 TEM equipped with a Gatan Model 894 2kX2k CCD camera.

Supplementary Material

Refer to Web version on PubMed Central for supplementary material.

ACKNOWLEDGMENTS

References

1. Butt AM, Jones HC, Abbott NJ. Electrical resistance across the blood-brain barrier in anaesthetized rats: a developmental study. The Journal of physiology. 1990; 429:47–62. [PubMed: 2277354]

2. Pardridge WM. Blood-brain barrier drug targeting: the future of brain drug development. Molecular interventions. 2003; 3:90–105. 151. [PubMed: 14993430]

3. Weiss N, Miller F, Cazaubon S, Couraud PO. The blood-brain barrier in brain homeostasis and neurological diseases. Biochimica et biophysica acta. 2009; 1788:842–857. [PubMed: 19061857]

4. Deli MA, Abraham CS, Kataoka Y, Niwa M. Permeability studies on in vitro blood-brain barrier models: physiology, pathology, and pharmacology. Cellular and molecular neurobiology. 2005; 25:59–127. [PubMed: 15962509]

5. Syvanen S, et al. Species differences in blood-brain barrier transport of three positron emission tomography radioligands with emphasis on P-glycoprotein transport. Drug metabolism and disposition: the biological fate of chemicals. 2009; 37:635–643. [PubMed: 19047468]

6. Warren MS, et al. Comparative gene expression profiles of ABC transporters in brain microvessel endothelial cells and brain in five species including human. Pharmacol Res. 2009; 59:404–413. [PubMed: 19429473]

7. Cecchelli R, et al. Modelling of the blood-brain barrier in drug discovery and development. Nat Rev Drug Discov. 2007; 6:650–661. [PubMed: 17667956]

8. Weksler BB, et al. Blood-brain barrier-specific properties of a human adult brain endothelial cell line. Faseb J. 2005; 19:1872–1874. [PubMed: 16141364]

9. Forster C, et al. Differential effects of hydrocortisone and TNFalpha on tight junction proteins in an in vitro model of the human blood-brain barrier. The Journal of physiology. 2008; 586:1937–1949. [PubMed: 18258663]

10. Man S, et al. Human brain microvascular endothelial cells and umbilical vein endothelial cells differentially facilitate leukocyte recruitment and utilize chemokines for T cell migration. Clinical & developmental immunology. 2008; 2008:384982. [PubMed: 18320011]

11. Thomson JA, et al. Embryonic stem cell lines derived from human blastocysts. Science (New York, N.Y. 1998; 282:1145–1147.

12. Takahashi K, et al. Induction of pluripotent stem cells from adult human fibroblasts by defined factors. Cell. 2007; 131:861–872. [PubMed: 18035408]

13. Yu J, et al. Induced pluripotent stem cell lines derived from human somatic cells. Science (New York, N.Y. 2007; 318:1917–1920.

14. Goldman O, et al. A boost of BMP4 accelerates the commitment of human embryonic stem cells to the endothelial lineage. Stem cells (Dayton, Ohio). 2009; 27:1750–1759.

15. James D, et al. Expansion and maintenance of human embryonic stem cell-derived endothelial cells by TGFbeta inhibition is Id1 dependent. Nature biotechnology. 28:161–166.

16. Levenberg S, Golub JS, Amit M, Itskovitz-Eldor J, Langer R. Endothelial cells derived from human embryonic stem cells. Proceedings of the National Academy of Sciences of the United States of America. 2002; 99:4391–4396. [PubMed: 11917100]

17. Nakahara M, et al. High-efficiency production of subculturable vascular endothelial cells from feeder-free human embryonic stem cells without cell-sorting technique. Cloning and stem cells. 2009; 11:509–522. [PubMed: 20025522]

18. Wang L, et al. Endothelial and hematopoietic cell fate of human embryonic stem cells originates from primitive endothelium with hemangioblastic properties. Immunity. 2004; 21:31–41. [PubMed: 15345218]

19. Choi KD, et al. Hematopoietic and endothelial differentiation of human induced pluripotent stem cells. Stem cells (Dayton, Ohio). 2009; 27:559–567.

20. Vodyanik MA, Bork JA, Thomson JA, Slukvin II. Human embryonic stem cell-derived CD34+ cells: efficient production in the coculture with OP9 stromal cells and analysis of lymphohematopoietic potential. Blood. 2005; 105:617–626. [PubMed: 15374881]

21. Cleaver O, Melton DA. Endothelial signaling during development. Nature medicine. 2003; 9:661–668.

22. Bauer H, et al. Ontogenic expression of the erythroid-type glucose transporter (Glut 1) in the telencephalon of the mouse: correlation to the tightening of the blood-brain barrier. Brain Res Dev Brain Res. 1995; 86:317–325. [PubMed: 7656423]

23. Bauer HC, et al. Neovascularization and the appearance of morphological characteristics of the blood-brain barrier in the embryonic mouse central nervous system. Brain Res Dev Brain Res. 1993; 75:269–278. [PubMed: 8261616]

24. Daneman R, Zhou L, Kebede AA, Barres BA. Pericytes are required for blood-brain barrier integrity during embryogenesis. Nature. 468:562–566. [PubMed: 20944625]

25. Stewart PA, Hayakawa K. Early ultrastructural changes in blood-brain barrier vessels of the rat embryo. Brain Res Dev Brain Res. 1994; 78:25–34. [PubMed: 8004771]

26. Daneman R, et al. Wnt/beta-catenin signaling is required for CNS, but not non-CNS, angiogenesis. Proceedings of the National Academy of Sciences of the United States of America. 2009; 106:641–646. [PubMed: 19129494]

27. Stenman JM, et al. Canonical Wnt signaling regulates organ-specific assembly and differentiation of CNS vasculature. Science (New York, N.Y. 2008; 322:1247–1250.

28. Ying QL, Stavridis M, Griffiths D, Li M, Smith A. Conversion of embryonic stem cells into neuroectodermal precursors in adherent monoculture. Nature biotechnology. 2003; 21:183–186.

29. Kane NM, et al. Derivation of endothelial cells from human embryonic stem cells by directed differentiation: analysis of microRNA and angiogenesis in vitro and in vivo. Arteriosclerosis, thrombosis, and vascular biology. 30:1389–1397.

30. Wang ZZ, et al. Endothelial cells derived from human embryonic stem cells form durable blood vessels in vivo. Nature biotechnology. 2007; 25:317–318.

31. Daneman R, et al. The mouse blood-brain barrier transcriptome: a new resource for understanding the development and function of brain endothelial cells. PloS one. 5:e13741. [PubMed: 21060791]

32. Calabria AR, Weidenfeller C, Jones AR, de Vries HE, Shusta EV. Puromycin-purified rat brain microvascular endothelial cell cultures exhibit improved barrier properties in response to glucocorticoid induction. Journal of neurochemistry. 2006; 97:922–933. [PubMed: 16573646]

33. Yu J, et al. Human induced pluripotent stem cells free of vector and transgene sequences. Science (New York, N.Y. 2009; 324:797–801.

34. Liebner S, et al. Wnt/beta-catenin signaling controls development of the blood-brain barrier. The Journal of cell biology. 2008; 183:409–417. [PubMed: 18955553]

35. Xu Q, et al. Vascular development in the retina and inner ear: control by Norrin and Frizzled-4, a high-affinity ligand-receptor pair. Cell. 2004; 116:883–895. [PubMed: 15035989]

36. Ye X, et al. Norrin, frizzled-4, and Lrp5 signaling in endothelial cells controls a genetic program for retinal vascularization. Cell. 2009; 139:285–298. [PubMed: 19837032]

37. Robitaille J, et al. Mutant frizzled-4 disrupts retinal angiogenesis in familial exudative vitreoretinopathy. Nature genetics. 2002; 32:326–330. [PubMed: 12172548]

38. Kawaguchi R, et al. A membrane receptor for retinol binding protein mediates cellular uptake of vitamin A. Science (New York, N.Y. 2007; 315:820–825.

39. Szeto W, et al. Overexpression of the retinoic acid-responsive gene Stra6 in human cancers and its synergistic induction by Wnt-1 and retinoic acid. Cancer research. 2001; 61:4197–4205. [PubMed: 11358845]

40. Shimomura Y, et al. APCDD1 is a novel Wnt inhibitor mutated in hereditary hypotrichosis simplex. Nature. 464:1043–1047. [PubMed: 20393562]

41. Anderson KD, et al. Angiogenic sprouting into neural tissue requires Gpr124, an orphan G protein-coupled receptor. Proceedings of the National Academy of Sciences of the United States of America. 108:2807–2812. [PubMed: 21282641]

42. Cullen M, et al. GPR124, an orphan G protein-coupled receptor, is required for CNS-specific vascularization and establishment of the blood-brain barrier. Proceedings of the National Academy of Sciences of the United States of America. 108:5759–5764. [PubMed: 21421844]

43. Kuhnert F, et al. Essential regulation of CNS angiogenesis by the orphan G protein-coupled receptor GPR124. Science (New York, N.Y. 330:985–989.

44. Vittet D, et al. Embryonic stem cells differentiate in vitro to endothelial cells through successive maturation steps. Blood. 1996; 88:3424–3431. [PubMed: 8896407]

45. Rubin LL, et al. A cell culture model of the blood-brain barrier. The Journal of cell biology. 1991; 115:1725–1735. [PubMed: 1661734]

46. Liebner S, Kniesel U, Kalbacher H, Wolburg H. Correlation of tight junction morphology with the expression of tight junction proteins in blood-brain barrier endothelial cells. European journal of cell biology. 2000; 79:707–717. [PubMed: 11089919]

47. Roberts LM, et al. Expression of the thyroid hormone transporters monocarboxylate transporter-8 (SLC16A2) and organic ion transporter-14 (SLCO1C1) at the blood-brain barrier. Endocrinology. 2008; 149:6251–6261. [PubMed: 18687783]

48. Uchida Y, et al. Quantitative targeted absolute proteomics of human blood-brain barrier transporters and receptors. Journal of neurochemistry. 117:333–345. [PubMed: 21291474]

49. Perriere N, et al. A functional in vitro model of rat blood-brain barrier for molecular analysis of efflux transporters. Brain Res. 2007; 1150:1–13. [PubMed: 17434463]

50. Cohen-Kashi Malina K, Cooper I, Teichberg VI. Closing the gap between the in-vivo and in-vitro blood-brain barrier tightness. Brain Res. 2009; 1284:12–21. [PubMed: 19501061]

51. Ludwig TE, et al. Feeder-independent culture of human embryonic stem cells. Nature methods. 2006; 3:637–646. [PubMed: 16862139]

52. Weidenfeller C, Svendsen CN, Shusta EV. Differentiating embryonic neural progenitor cells induce blood-brain barrier properties. Journal of neurochemistry. 2007; 101:555–565. [PubMed: 17254017]

53. de Planell-Saguer M, Rodicio MC, Mourelatos Z. Rapid in situ codetection of noncoding RNAs and proteins in cells and formalin-fixed paraffin-embedded tissue sections without protease treatment. Nature protocols. 5:1061–1073. [PubMed: 20539282]

54. Huang SM, et al. Tankyrase inhibition stabilizes axin and antagonizes Wnt signalling. Nature. 2009; 461:614–620. [PubMed: 19759537]

55. Dravid G, et al. Defining the role of Wnt/beta-catenin signaling in the survival, proliferation, and self-renewal of human embryonic stem cells. Stem cells (Dayton, Ohio). 2005; 23:1489–1501.

56. Tuomi JM, Voorbraak F, Jones DL, Ruijter JM. Bias in the Cq value observed with hydrolysis probe based quantitative PCR can be corrected with the estimated PCR efficiency value. Methods (San Diego, Calif. 50:313–322.
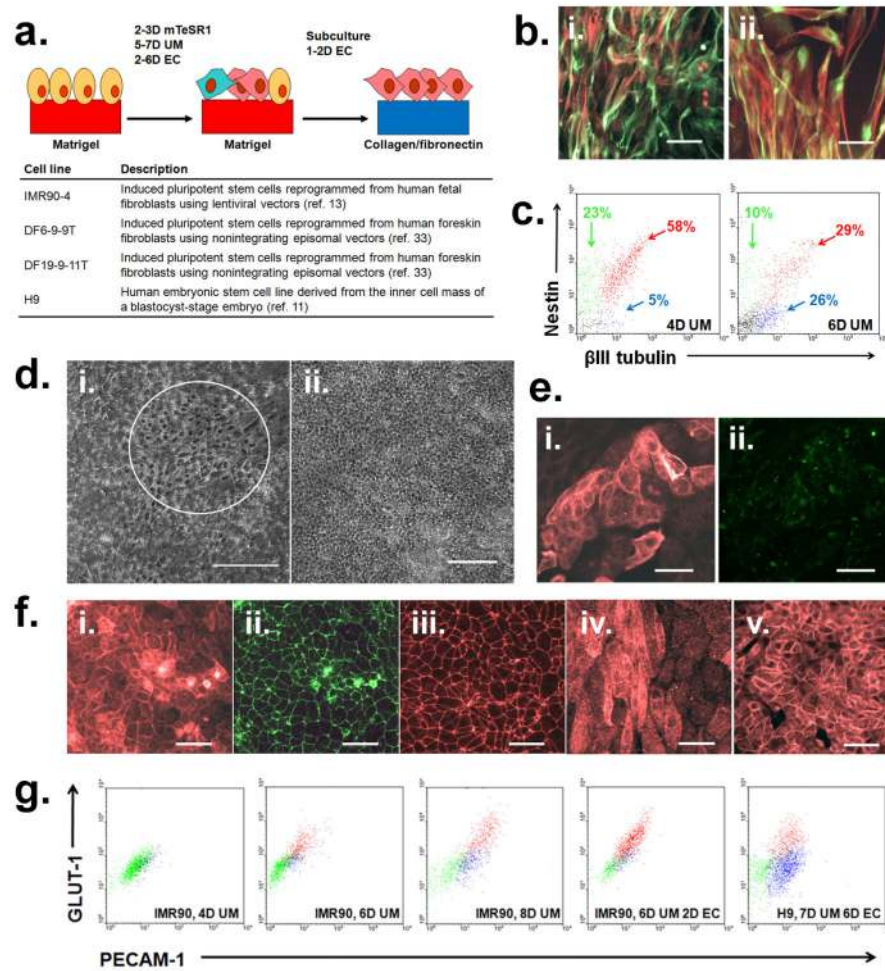
Figure 1. Differentiation of hPSCs to BMECs

(a) Schematic of BMEC differentiation protocol. hPSCs are seeded onto Matrigel in mTeSR1 medium for 2-3 days to allow adherence and cell expansion, then cultured in unconditioned medium for 5-7 days until large colonies with characteristic endothelial cell (EC) morphology are observed. Addition of defined EC medium for 2-6 days facilitates EC expansion prior to subculture onto a collagen/fibronectin matrix for further expansion and purification. iPSC and hPSC lines used in this study and their descriptions are listed. UM = unconditioned medium, EC = endothelial cell medium. (b) βIII tubulin (red) and nestin (green) expression is detected after differentiation of IMR90-4 iPSCs in UM for 4 days (panel i) and 6 days (panel ii). Scale bars indicate 50 μm. (c) Flow cytometric distributions of IMR90-4-derived βIII tubulin+ and nestin+ cells at day 4 and day 6 of UM treatment. Red dots indicate βIII tubulin+/nestin+ cells, blue dots indicate βIII tubulin+/nestin− cells, green dots indicate βIII tubulin−/nestin+ cells, and black dots indicate βIII tubulin−/nestin− cells. The data are representative of two biological replicates. (d) Phase contrast image of IMR90-4 iPSCs after 3 days in UM (panel i) and 6 days in UM with 3 additional days in EC medium (panel ii). The circle in panel i indicates a small region with flattened cobblestone EC morphology and is the type of region probed with antibodies in panel 1e. This

morphology is shown to be widespread in panel ii and corresponds to the regions identified by immunolabeling in Figure 1f and Supplementary Figure 3. Scale bars indicate 200 μm. (e) IMR90-4 iPSCs cultured for 4 days UM give rise to PECAM-1^{+} cells (panel i) that do not express tight junction protein claudin-5 (panel ii). Scale bars indicate 50 μm. (f) After 5-7 days of UM treatment, IMR90-4-derived ECs now co-express PECAM-1 (panel i, red) and claudin-5 (panel ii, green, same field). Within these EC colonies, expression of characteristic BBB markers occludin (panel iii), p-glycoprotein (panel iv), and GLUT-1 (panel v) is also observed. All scale bars indicate 50 μm. (g) Flow cytometry dot plots demonstrate the temporal evolution of the PECAM-1^{+}/GLUT-1^{+} population within differentiating IMR90-4 iPSCs or H9 hESCs. Green dots indicate PECAM-1^{−}/GLUT-1^{−} cells, blue dots indicate PECAM-1^{+}/GLUT-1^{−} cells, and red dots indicate PECAM-1^{+}/ GLUT-1^{+} cells. Full quantitative results are found in Table 1.
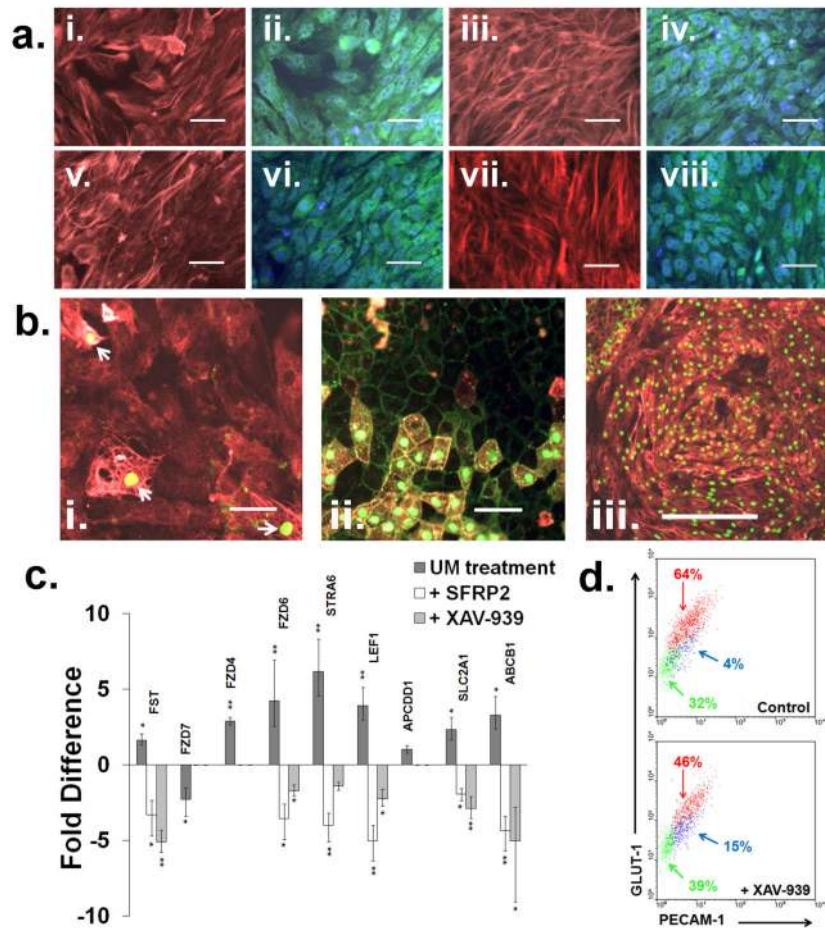
Figure 2. Wnt/β-catenin signaling involvement in BBB specification from hPSCs

(a) Combined fluorescence *in situ* hybridization/immunocytochemistry of IMR90-4 cultures at day 4 of UM treatment shows nestin$^+$ (red; panels i and v) and βIII tubulin$^+$ (red; panels iii and vii) cells express both *WNT7A* (green; panels ii and iv) and *WNT7B* (green; panels vi and viii). *WNT7A/7B* are shown overlaid with DAPI nuclear stain (blue). Panels i and ii, iii and iv, v and vi, and vii and viii are the same field. Scale bars indicate 50 μm. (b) Nuclear β-catenin localization increases with differentiation time. Nuclear β-catenin (green) is sparsely observed in IMR90-4-derived PECAM-1$^+$ (red) EC clusters after 4 days of UM treatment (panel i). Arrowheads indicate nuclear β-catenin. Nuclear β-catenin localization (green) increases after 5 days of UM treatment (panel ii) and elevated GLUT-1 (red) is only observed elevated in cells that also have nuclear β-catenin. After 6 days of UM and 2 days of EC medium treatment (panel iii), nuclear β-catenin (green) is co-localized with the majority of PECAM-1$^+$ cells (red). Scale bars in panel i and panel ii indicate 50 μm and scale bar in panel iii indicates 100 μm. (c) Quantitative RT-PCR comparing fold difference gene expression in differentiating IMR90-4 iPSCs demonstrates that Wnt-activated gene expression is temporally correlated with the observed time course of BBB differentiation. The dark bars compare IMR90-4 cells treated with UM for 3 days and 7 days. A positive fold difference represents gene upregulation at 7 days of UM treatment. The white bars indicate IMR90-4 cells treated with UM containing SFRP2 for 7 days. A negative fold

difference represents a downregulation of gene transcription in cells treated with UM containing SFRP2 compared to cells only treated with UM. The grey bars indicate IMR90-4 cells treated with XAV-939 from days 2 thru 7 of UM treatment compared to cells treated with DMSO vehicle control. *FZD4, FZD7*, and *APCDD1* expression were not tested in the presence of inhibitors. Error bars indicate standard deviation calculated from triplicate samples. Data are representative of two biological replicates. Statistical analysis was performed using Student's unpaired t-test; *****, $p<0.05$; ******, $p<0.005$. (d) Flow cytometry of IMR90-4 cells at 6 days of UM and 2 days of EC medium treatment after addition of XAV-939 or DMSO vehicle control starting at day 2 of UM treatment. Cells treated with DMSO show similar distribution to untreated cells (64% PECAM-1$^+$/GLUT-1$^+$ and 68% PECAM-1$^+$ overall; Table 1). Cells treated with XAV-939 show a small reduction in overall PECAM-1$^+$ labeling (61% total) and a marked decrease in the number of PECAM-1$^+$/GLUT-1$^+$ cells (46% total) (Table 1). Red dots indicate PECAM-1$^+$/GLUT-1$^+$ cells, blue dots indicate PECAM-1$^+$/GLUT-1$^-$ cells, and green dots indicate PECAM-1$^-$/GLUT-1$^-$ cells. The results are representative of three biological replicates.
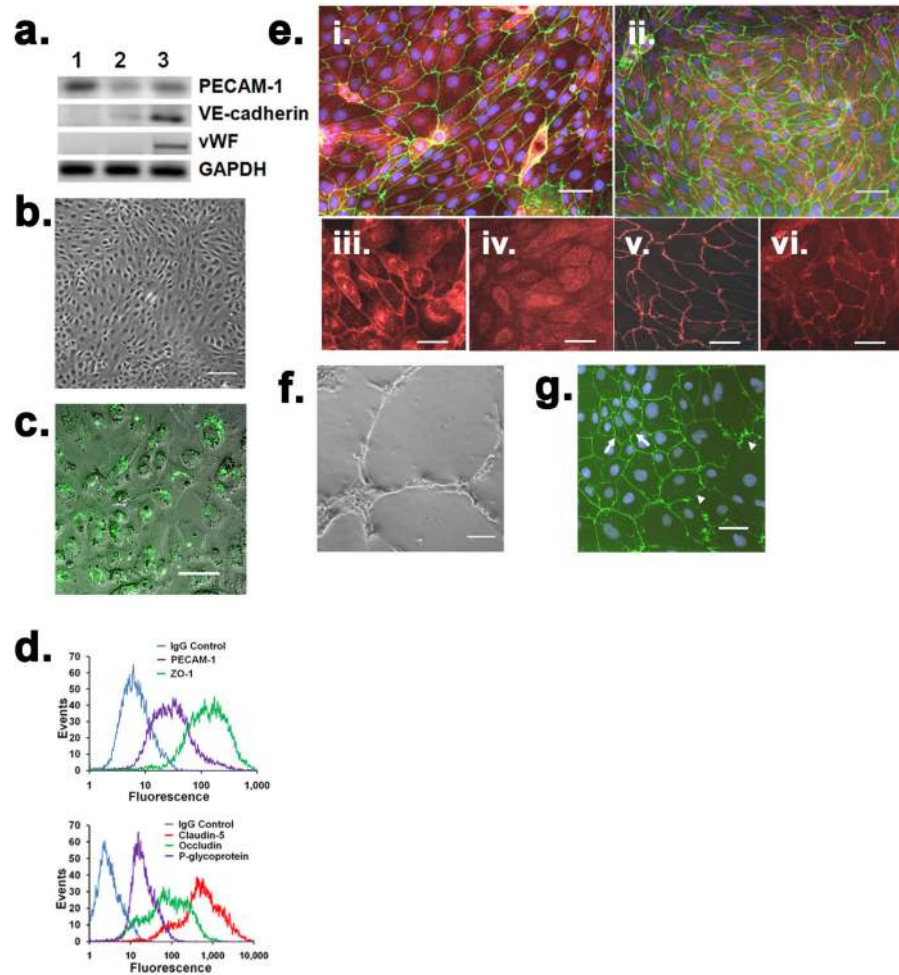
Figure 3. Purification of iPSC-derived BMECs on collagen/fibronectin matrix
(a) Gel electrophoresis of RT-PCR products for transcripts encoding PECAM-1, VE-cadherin, and von Willebrand Factor (vWF) in differentiating IMR90-4 iPSCs after 3 days of differentiation in UM (lane 1), 6 days in UM and 2 days in EC medium (lane 2), or subculture onto a collagen/fibronectin matrix for 2 days (lane 3). (b) Phase contrast image of IMR90-4-derived BMECs on the collagen/fibronectin matrix. Scale bar indicates 100 μm. (c) IMR90-4-derived BMECs were capable of fluorescent acetylated LDL uptake (scale bar indicates 50 μm). (d) Flow cytometry demonstrates purity of IMR90-4-derived BMECs after subculture. ZO-1 and PECAM-1 expression are compared to the appropriate rabbit IgG control, and occludin, claudin-5, and p-glycoprotein expression are compared to the appropriate mouse IgG control in the flow cytometric histograms. (e) Characteristic EC and BBB markers are expressed by purified IMR90-4-derived BMECs. IMR90-4-derived BMECs express PECAM-1 (panel i; red), claudin-5 (panel i; green), vWF (panel ii; red), occludin (panel ii; green), GLUT-1 (panel iii), p-glycoprotein (panel iv), ZO-1 (panel v), and VE-cadherin (panel vi). DAPI nuclear stain (blue) is overlaid in panels i and ii. Scale bars indicate 50 μm. (f) Seeding of purified IMR90-4-derived BMECs onto Matrigel in the presence of 40 ng/mL VEGF leads to vascular tube formation (scale bar indicates 100 μm). In the absence of VEGF, cells did not form tubes. (g) Subculture prior to full differentiation

leads to a defective BBB phenotype. Differentiating IMR90-4 cultures purified on the collagen/fibronectin matrix after only 4 days of UM treatment do not grow to confluence and areas with malformed or discontinuous claudin-5 expression (green) are readily observed. Co-label with DAPI is shown (blue). Arrows highlight continuous claudin-5 expression while arrowheads indicate defective claudin-5. Scale bar indicates 50 μm.
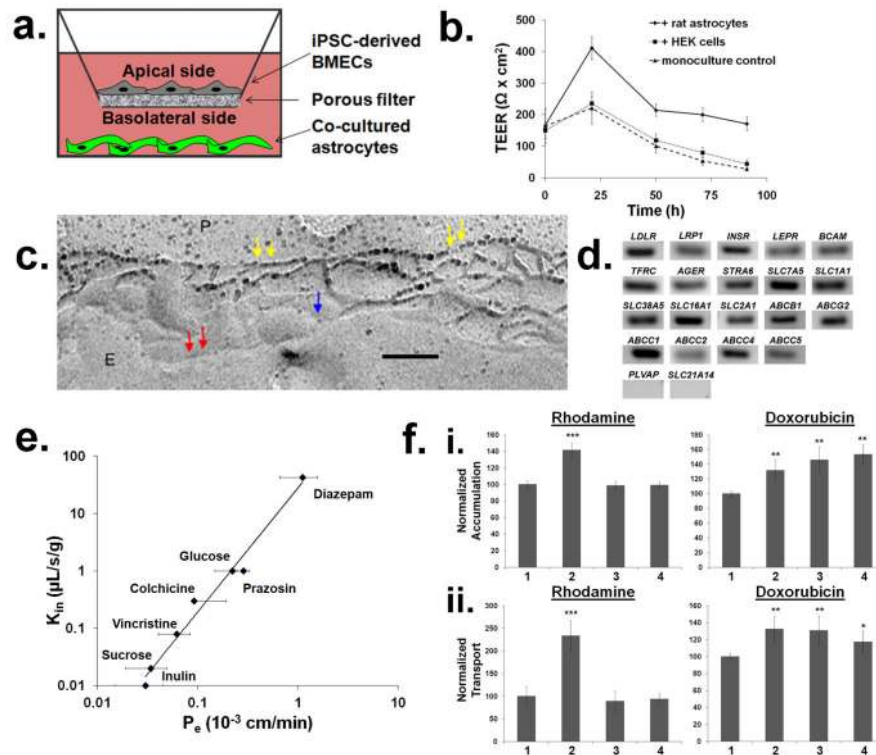
Figure 4. Functional barrier properties and BBB characteristics of purified iPSC-derived BMECs

(a) Schematic of a two-compartment blood-brain barrier model. iPSC-derived BMECs are seeded onto a Transwell filter coated with collagen/fibronectin and co-cultured with rat astrocytes to assay for induction of BBB properties. Apical (blood side) and basolateral (brain side) chambers are denoted with respect to the transport assays. (b) iPSC-derived BMECs respond to soluble cues from astrocytes. IMR90-4-derived BMECs were cultured alone (monoculture) or co-cultured with either rat astrocytes or human embryonic kidney (HEK) cells for 96 hours and trans-endothelial electrical resistance (TEER) was monitored. Error bars represent standard deviation of triplicate filters. The preferential TEER response due to astrocyte co-culture compared to HEK co-culture was observed for more than ten biological replicates. See Table 2 for TEER values from experiments with optimized medium and seeding density. (c) Freeze-fracture electron microscopy of IMR90-4-derived BMECs after co-culture with rat astrocytes for 24 hours. "P" indicates protoplasmic face (P-face) and "E" indicates exocytoplasmic face (E-face). Red arrowheads indicate an E-face groove largely devoid of tight junction particles, blue arrowhead highlights an infrequent tight junction particle found at the E-face and the yellow arrowheads indicate the complex network of tight junction particles associated with the P-face. Scale bar indicates 0.2 μm. (d) RT-PCR detection of representative blood-brain barrier transcript expression in IMR90-4-derived BMECs co-cultured with rat astrocytes. Transcript presence was confirmed for LDLR, LRP1, INSR, LEPR, BCAM, TFRC, AGER, STRA6, SLC7A5, SLC1A1, SLC38A5, SLC16A1, SLC2A1, ABCB1, ABCG2, ABCC1, ABCC2, ABCC4, and *ABCC5*. *PLVAP* and *SLC21A14* transcripts were not detected. Monocultured IMR90-4-derived

BMECs had a similar transcript profile except *LRP1* and *ABCC5* were absent, requiring co-culture with either HEK293 cells or astrocytes for their induction. (e) Correlation between IMR90-4-derived BMEC permeability coefficients (P_e, x-axis) and rodent *in vivo* transfer coefficients (K_{in}, y-axis). P_e values (cm/min) were calculated from flux experiments using triplicate filters as described in the Material and Methods section. Depicted are the mean ± S.D. values generated for each compound measured in at least three such experiments. To accumulate these data, five individual co-culture models (independently differentiated from undifferentiated iPSCs) were assembled and 3-6 compounds measured at a time. Sucrose P_e values were also acquired from efflux transporter inhibition assay controls. Thus, the plot accurately depicts the biological variation in P_e measurements amongst completely independent experiments. Colchicine was the only compound having large variability across biological replicates (see Supplementary Table 1 for numerical values). K_{in} values ($\mu L\ s^{-1}\ g^{-1}$) were extracted from plotted *in situ* rodent brain perfusion data reported in Perriere *et al*[49]. (f) Functional expression of efflux transporters in IMR90-4-derived BMECs. Accumulation of rhodamine 123 or [^{14}C]-doxorubicin into monocultured IMR90-4-derived BMECs was measured in the presence and absence of cyclosporin A, Ko143, or MK 571 (panel i). Transport of rhodamine 123 or doxorubicin from the apical to basolateral chambers was measured in the two compartment astrocyte co-culture model in the presence and absence of cyclosporin A, Ko143, or MK 571 (panel ii). For all plots, Lane 1 = control, Lane 2 = cyclosporin A addition, Lane 3 = Ko143 addition, Lane 4 = MK 571 addition. Error bars indicate standard deviation calculated from triplicate wells or filters. Data are representative of two biological replicates for each inhibition assay. Statistical significance was calculated by Student's unpaired t-test; ***, $p<0.01$; **, $p<0.05$; *, $p<0.1$.

Table 1

Quantitative assessment of hPSC-derived BMEC differentiation

IMR90-4 cell line

Differentiation time[a]	% GLUT-1$^+$/PECAM-1$^+$	% PECAM-1$^+$ overall	Mean per cell expression of GLUT-1[b] (A.U.)
4D UM	0	5	N/A
6D UM	30	36	99
6D UM 1D EC	36	42	221
6D UM 2D EC	66	68	300
6D UM 2D EC (+10μM XAV-939)	46	61	272
6D UM 2D EC (+DMSO control)	64	68	285
8D UM	39	61	263
C/F[c]	100	100	553

DF19-9-11T cell line

Differentiation time[a]	% GLUT-1$^+$/PECAM-1$^+$	% PECAM-1$^+$ overall	Mean per cell expression of GLUT-1[b] (A.U.)
6D UM 2D EC	75	75	70
C/F[c]	100	100	76

H9 cell line

Differentiation time[a]	% GLUT-1$^+$/PECAM-1$^+$	% PECAM-1$^+$ overall	Mean per cell expression of GLUT-1[b] (A.U.)
6D UM 2D EC	16	41	110
7D UM 6D EC	35	63	109

Percentages are representative of at least two independent biological replicates.

[a] Refers to time in unconditioned medium (UM), followed by time in EC medium (EC).

[b] Mean per cell expression of GLUT-1 in arbitrary units as measured by flow cytometry. Baseline values for GLUT-1 are different for each line tested, and thus should not be used for comparison between different hPSC lines.

[c] Refers to cells subcultured on fibronectin/collagen IV and grown to confluence.

Table 2

Evaluation of iPSC-derived BMEC TEER.

Co-cultured cell	Co-culture medium[a]	Maximum TEER ($\Omega \times cm^2$)[b]
IMR90-4-derived BMECs		
Monoculture	1% PDS	222 ± 51
HEKs	1% PDS	236 ± 23
HEKs	10% FBS	364 ± 53
HEKs (optimized)[c]	10% FBS	899 ± 132
Astrocytes	1% PDS	412 ± 38
Astrocytes	10% FBS	696 ± 8
Astrocytes (optimized)[c]	10% FBS	1450 ± 140
DF19-9-11T-derived BMECs		
Astrocytes (optimized)[c]	10% FBS	777 ± 112

[a]Refers to serum component of culture media. Full media details found in Materials and Methods. 1% PDS = EC medium.

[b]Measured at approximately 24 hours of co-culture. TEER is expressed as mean ± standard deviation measured from triplicate filters.

[c]Refers to optimized BMEC subculture density to reduce nonspecific cell adherence and debris accumulation.